IOP Publishing Journal of Physics: Condensed Matter
J. Phys.: Condens. Matter **32** (2020) 355003 (12pp) https://doi.org/10.1088/1361-648X/ab8251

First-principles study of the ferroelectric properties of $SrTaO_2N/SrTiO_3$ interfaces

R C Bastidas Briceño[1,2], V I Fernández[2,3] and R E Alonso[1,2,4]

[1] Departamento de Ciencias Básicas, Facultad de Ingeniería Universidad Nacional de La Plata, La Plata, Argentina
[2] Instituto de Física La Plata (IFLP), CONICET, Argentina
[3] Departamento de Física, Facultad de Ciencias Exactas, Universidad Nacional de La Plata, Argentina
[4] Instituto de Ingeniería y Agronomía, Universidad Nacional Arturo Jauretche, Argentina

E-mail: victoria@fisica.unlp.edu.ar

Received 23 December 2019, revised 26 February 2020
Accepted for publication 23 March 2020
Published 3 June 2020

Abstract

First-principles calculations based on density–functional theory in the pseudo-potential approach have been performed for the total energy, crystal structure and cell polarization for $SrTaO_2N/SrTiO_3$ heterostructures. Different heterojunctions were analyzed in terms of the termination atoms at the interface plane, and periodic or non-periodic stacking in the perpendicular direction. The calculations show that the $SrTaO_2N$ layer is compressed along the *ab*-plane, while the $SrTiO_3$ is elongated, thus favoring the formation of *P*4*mm* local environment on both sides of the interface, leading to net macroscopic polarization. The analysis of the local polarization as a function of the distance to the interface, for each individual unit cell was found to depend on the presence of a N or an O atom at the interface, and also on the asymmetric and not uniform *c*-axis deformation due to the induced strain in the *ab*-plane. The resulting total polarization in the periodic array was ≈ 0.54 C m^{-2}, which makes this type of arrangement suitable for microelectronic applications.

Keywords: *ab initio* calculations, ferroelectrics, heterostructures

Supplementary material for this article is available online

(Some figures may appear in colour only in the online journal)

1. Introduction

In nature there exist several compounds with chemical formula ABO_3 and perovskite structure (for example A = Ca, Pb, Sr, Ba or lanthanide, B = Ti, Hf, Zr, Ta or Nb). Depending on the A and B combinations, compounds with highly desirable physical properties have been found, such as ferromagnetism, ferroelectricity, piezoelectricity, superconductivity and giant magneto-resistance [1]. In the last decades these materials have been widely investigated due to their scientific and technological interesting properties, and at the same time leading these materials to widespread use in microelectronics. Some of them present drastic anomalies in their dielectric constant at a given temperature that indicate the occurrence of a phase transition, for example, a paraelectric to ferroelectric or paraelectric to antiferroelectric phase transition. On the other hand, in recent years a modification of these compounds, the $AB(O,N)_3$ oxynitrides, has attracted much attention due to their own electronic functionalities, such as visible light absorption [2], high dielectric constant [3], photocatalytic activity and colossal magneto-resistance [4, 5]. They can be built performing partial substitution of oxygen by nitrogen atoms into the anionic network of the ABO_3 perovskites. The increment of negative charge is compensated with cationic replacement in the B site (for example Ti by Ta) [6–9]. The replacement of O by N changes the band-gap, and then, the color of the initially white powders. In this way, oxynitrides have potential use as safe colored pigment materials that can replace currently used pollutants heavy metals (Cr, Cd, Pb, etc) [2]. The change in the resulting optical

properties is correlated with the changes in the oxygen bonding and the internal structure due to the partial oxygen substitution, which also gives rise to new and promising dielectric behavior. The aliovalent substitution provides a mechanism for enhancing the dielectric polarizability through the substitution of more polarizable ions into the lattice [10]. The lower electronegativity of the nitrogen atom with respect to the oxygen tends to increase the covalency of the cation–anion bonds [3]. This in turn increases the cation displacements through a second-order Jahn–Teller distortion of the d^0 cation [11–13]. And such displacements are in many cases associated with the origin of ferroelectricity. In $AM(O_{1-x}N_x)_3$ oxynitrides, the mixed occupancy of the anion sites can lead the polarized octahedral cations to be surrounded by random chemical environments due to the absence of a complete O/N ordering. This fact provides the conditions to form a relaxor material. It is, therefore, an interesting issue to examine whether the oxynitride perovskites possess intrinsically high κ and relaxor-like properties.

The electronic properties of perovskite oxynitrides will be influenced by the geometrical configuration of the O and N atoms around their central cations. In ABO_2N-type oxynitrides, B cations are surrounded by four O and two N ions, forming a BO_4N_2 octahedron. In each octahedron, there are two possible anion configurations: the two nitrogen ions can occupy either adjacent (cis-type) or opposite (trans-type) sites. Several recent studies argued that the dielectric properties of ABO_2N are related to anion arrangement: Page *et al* suggested that ferroelectricity in trans-type anion-ordered $ATaO_2N$ (A = Sr, Ba) phases may be caused by the off-center displacement of Ta ions [14]. In their work, this concept is achieved by the theoretical study of the stability of phases with different nitrogen arrangements and space groups. However, it has been stated that trans-type phases in this system are energetically less stable than cis-type phases, and bulk $SrTaO_2N$ (STN) specimens have been confirmed to exhibit cis-type configurations in an *I*4*mcm* centro-symmetric space group [15, 16]. However, different ferroelectric and relaxor regions were recently detected in thin films samples of STN epitaxially grown on a $SrTiO_3$ (STO) substrate [17, 18]. The lattice mismatch between the compound and the substrate produces strain on the oxynitride in the plane parallel to the interface, thereby reducing the in-plane lattice constant when it is grown as thin film. This induced strain favors the stabilization of a trans-type non-centro-symmetric polar *P*4*mm* ferroelectric structure [14, 17]. Also, Haeni *et al* suggested that strain and substrate clamping induce in epitaxial STO films structures that are not present on the bulk material. For the case of tensile strain, a phase transition from the tetragonal *P*4*mm* high temperature phase to the orthorhombic *Cmcm* low temperature phase may occur [19].

Computational quantum simulations have proven to be a suitable tool for understanding the microscopic processes that drive the physical properties of materials. Despite the simplifications that are made to model the systems taking into account the complexity of real materials (especially in disordered and ceramic materials), they can lead to a better understanding of the individual processes involved. Some previous studies on phase stability in bulk-strained STN and STO have been published [14, 17, 19–21]. Nevertheless, the behavior of the $SrTiO_3/SrTaO_2N$ interface opens new questions regarding the mutually induced strain and cell deformations, together with the possible coupling of the dipole moments above and below the interface. The bulk lattice mismatch (a_{STO} = 3.905 Å, a_{STN} = 4.0271 Å) produces a tensile strain for the STO layer and a compressive strain on the STN layer when the interface is formed. Accordingly, both compounds could stabilize in the ferroelectric *P*4*mm* phase. In this work, we study different configurations of $SrTiO_3/SrTaO_2N$ interfaces within the density functional theory (DFT) [22]. We will analyze the ferroelectric distortion in the tetragonal induced *P*4*mm* phases above and below the interface, due to compressive strain on the side of $SrTaO_2N$ and tensile strain corresponding to the $SrTiO_3$, in order to compute the resulting net dipole moment. The paper is organized as follows: in section 2 the method used for calculations is described. In section 3 the configurations of the different considered interlayers are explained. In section 4 the comparative results of the calculations of the pure STN and STO vs. the SCs systems are shown. In section 5 a detailed analysis of the cell and sub-cell polarization is presented. Finally, in section 6 the summary and conclusions are discussed. Also, we include supplementary information with the details of the atomic positions and polarization contributions per atom for the different SCs under study (https://stacks.iop.org/JPCM/32/355003/mmedia).

2. Method of calculation

Ab initio electronic structure calculations were used to determine the self-consistent potential and the charge density of the different configurations analyzed, and from these first-principles calculations, the cell polarization was obtained. The calculations have been performed using the QUANTUM ESPRESSO code [23], which is based on the density functional theory (DFT) [22].

For the electronic exchange-correlation potential the generalized gradient approximation (GGA) based on the Perdew–Burke–Ernzerhof expression was used [24]. The electron–ion interaction was treated by using Vanderbilt ultrasoft pseudopotentials [25], with the following valence electronic configuration, $Sr(4s^25s^24p^65p^0)$, $Ti(3s^24s^23p^64p^03d^2)$, $Ta(5s^26s^25p^66p^05d^3)$, $N(2s^22p^3)$ and $O(2s^22p^4)$. Wave functions were expanded by plane waves with a kinetic energy cut-off of 75 Ry and an energy cut-off of 600 Ry for the charge density. The irreducible Brillouin zone was sampled using the Monkhorst–Pack scheme with a $6 \times 6 \times 1$ mesh [26]. In order to calculate the density of states (DOS) the tetrahedron method has been used with a denser $20 \times 20 \times 5$ mesh [27], whereas the atomic-projected DOS were calculated by the Lowdin populations [28]. The equilibrium structure for each case was obtained through ionic relaxations performed until the residual forces on the ions were less than 10 meV Å^{-1} with a Broyden, Fletcher, Goldfarb and Shanno algorithm, and a pressure convergence threshold of 0.5 kBar for the cell. For the analysis of the ionic and electronic contribution to the polarization, the modern theory of polarization formalism according

to King-Smith and Vanderbilt [29], and the Born's effective charge tensor method were used [30, 31].

In order to check the reliability of this theoretical approach and the applicability of the selected pseudopotentials, the method was first applied to determine the well-established properties of pure bulk STN and STO (see section 4). The obtained results were compared with calculations performed using the all-electron full-potential linear augmented plane wave plus local orbital (FP_APW) method in the scalar relativistic version [32–34], with the WIEN2k implementation [35], using the same exchange-correlation potential. For the WIEN2k calculations, the energy cut-off criterion was $R_{\mathrm{mt}}K_{\max} = 8$ for the system (R_{mt} denotes the smallest muffin-tin radius and $K_{\max}$ the largest wave number of the basis set). Integration in reciprocal space was performed using the tetrahedron method, considering 300 k-points in the full Brillouin zone (BZ), which are reduced to 10 k-points in the irreducible wedge of the BZ (IBZ).

3. The system under study

Bulk STN have been reported to exhibit cis-type configuration with $I4mcm$ space group at room temperature (RT), with lattice constants $a = 5.70251(6)$ Å and $c = 8.05420(16)$ Å (using the pseudo-cubic parameters $a \approx 4.032$ Å and $c \approx 4.0271$ Å [3]). On the other hand, at room temperature STO crystallizes in the simple cubic perovskite structure with space group $Pm3m$ and lattice parameter 3.905 Å. For an interface made of a STN thin film over a STO substrate, a substantial lattice mismatch (3.28%) exists during hetero-epitaxial deposition due to the difference in the in-plane lattice constants. As a result, the substrate becomes subjected to high tensile strain, which in turn may cause an alteration of the lattice symmetry of STO from cubic to tetragonal, and this results in the consequent appearance of Raman-inactive first-order phonons [18]. Also, at the STN side, a compressive epitaxial stress may stabilize a ferroelectric trans-type $P4mm$ phase, as suggested by Page *et al* [14].

Lattice mismatch can lead to misfit dislocations and other microstructural features, such as secondary phases, interfacial defects, changes in the stoichiometry of the component materials, cation intermixing across the interface, stacking faults, and others, to alleviate the strain. All these features can change the physics of the interface, in particular, the affected sub-cells polarization. In reference [36], in particular it is stated that if the misfit strain is relatively small (lower than 7%–8%), it can be accommodated by the materials, and coherency can be achieved. Yet, it is known that the misfit percentage tolerance will vary with the film thickness, the method of deposition, and the particular specimens forming the heterostructure. Few years ago STN/STO interfaces were successfully built with STN thin film format onto a STO substrate, despite the difference in lattice constants between them [17, 18]. In both works, N-assisted pulsed laser deposition method was employed for the film formation. This is an out-of-equilibrium deposition technique. Figure 2(d) in [17] shows a cross sectional TEM image of the interface. It can be observed a clean $SrTaO_2N/SrTiO_3$ interface. And in figure 2(e) in [17] a uniform perovskite lattice structure with no segregation is shown. Although the interface looks fine, there are no further experimental analysis of the presence of dislocations and defects that can been expected under such lattice mismatch. In the cited work, the characteristics of the thin film are also analyzed according to the nitrogen content, and XRD analysis of the sample structures are performed, determining a tetragonal structure for all the compositions. Also, ferroelectric domains are observed, and the origin of this phenomenon is attributed to the deformation suffered by the STN due to the compression effort given by epitaxial growth.

In this work, the experimental situations mentioned above were modeled by building two different heterostructure formats:

First, n layers of STN over n layers of STO in the (001) direction are arranged. This structure, due to the periodic boundary conditions, forms an infinite multilayer that allows to analyze the tension/compression effect, the induced electrical polarization and its dependence with the distance to the interface. In order to study the electrical polarization induced by the tensile (compression) stress in STO (STN) as a function of the distance of the respective sub-cell unit to the interface plane, supercells (SCs) were made with different sizes and configurations. The aim is to study each individual perovskite sub-cell structure. Thus, n-$SrTaO_2N$/n-$SrTiO_3$ SCs with $n = 3$, 4 and 5 were constructed (30, 40 and 50 atoms in the structure respectively). An example of these structures for $n = 4$ can be observed in figure 1 (above). As already mentioned, periodic boundary condition transforms this geometry in a periodic multilayer …/STN/STO/STN/… with planar interfaces. If the interface is constructed along the ab-plane at the Sr atoms level, then, in the center of the four Sr square plane there will be either an O or a N atom. If there is an O atom (SrO interface-type), the STO sub-cell just above the interface has a normal TiO_6 octahedron, whereas the STN sub-cell immediately below the interface has a TaO_5N octahedron (see figure 2(a)). In order to maintain the stoichiometry, at the next interface, generated by the periodic boundary conditions, there will be a N atom in the middle of the Sr square (SrN interface-type) (see figure 2(b)). Thus, the STO sub-cell immediately below the interface has a TiO_5N octahedron and the STN sub-cell just above has a TaO_4N_2 octahedron, being this last the configuration for trans-type oxynitrides. Therefore, this periodic multilayer array allows the analysis of the electronic behavior of the two types of interface-termination cases (SrO and SrN) simultaneously.

On the other hand, in order to approximately model the effect of a single thin layer on a substrate as in the experiment of reference [17], a different heterostructure formed by stacking n layers of STN on m layers of STO, with $m > n$ (figure 1 (below)) was also built. This last structure contains a vacuum separator layer to ensure that the periodic boundary conditions have a negligible effect. Thus, the V/n-$SrTaO_2N$/m-$SrTiO_3$ cells were built, with $n \times m = 4 \times 8$ and 5×10 (figure 1 (below)). These SCs have twice the unit formulas of STO with respect to those of STN, and the V vacuum separator layer thick is 10 Å in the (001) direction (60 and 75 atoms in the

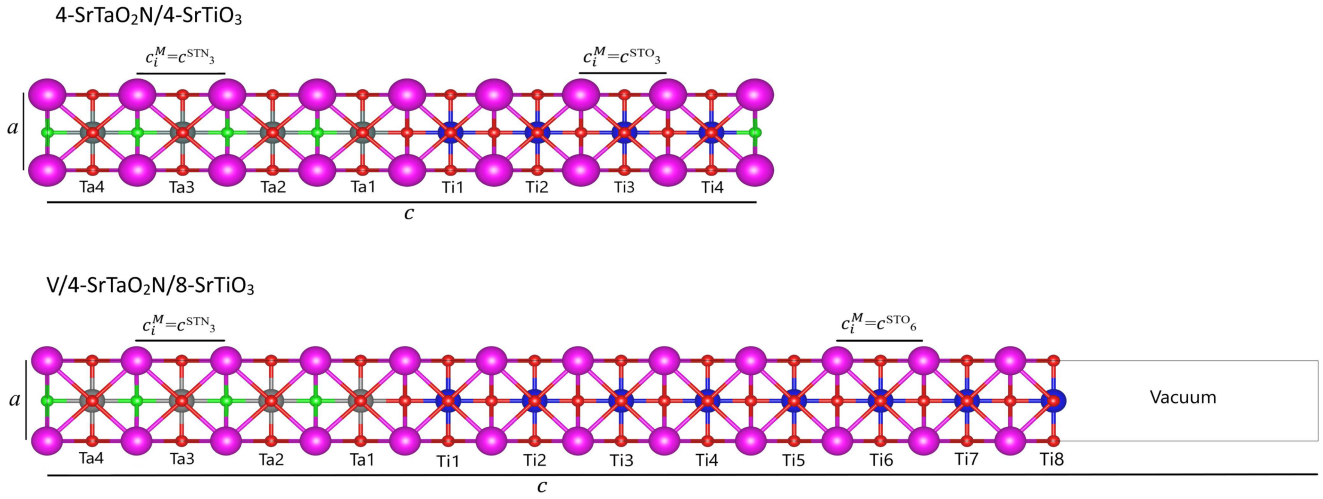

Figure 1. Schematic atomic distribution in 4-$SrTaO_2N$/4-$SrTiO_3$ (above) and V/4-$SrTaO_2N$/8-$SrTiO_3$ (below) SCs.

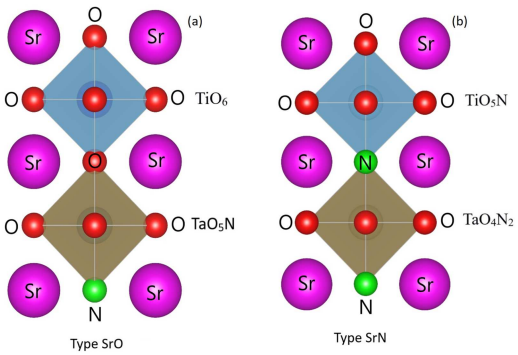

Figure 2. Detailed view of the different termination modes at the interface (central horizontal Sr's plane). SrO-type termination corresponds to TaO_5N/TiO_6 octahedra (a), while SrN-type termination corresponds to TaO_4N_2/TiO_5N octahedra (b).

structure respectively). The vacuum layer prevents the induction of dipole moments and strain in the STO layer from below by the STN layer due to periodicity, as it occurs in the previous multilayer scheme. To determine the thickness of the vacuum layer, the final positions of the atoms after relaxation were studied for different increasing thicknesses of vacuum, until the differences in the atomic positions were less than 0.001 Å. In addition, the greater number of STO sub-cells compared with those of STN, better reflects the experimental situation mentioned [17]. The V/*n*-$SrTaO_2N$/*m*-$SrTiO_3$ SCs were built with two types of possible terminations at the interface, that is, with an O or a N atom at the separation plane of the interface (corresponding to SrO or SrN-type respectively) (figure 2).

For all the SCs in this work, an initial tetragonal configuration was used for both layers, where the initial lattice constant *a* has been chosen as an intermediate value of the corresponding to bulk STO and STN. For the STO layer, the initial positions were selected as a centro-symmetric configuration (4/*mmm*), whereas for the STN layer, a non-centro-symmetric (4/*mm*) configuration was selected, being the Ta atoms slightly displaced outside of the symmetry plane. All the initial sub-cells of each layer were built with the same configuration. From these initial configurations, the whole atomic positions and cell constants were relaxed, as described in section 2.

Tests were performed with a different arrangement of the N atoms in the STN shell: trans-type N atoms parallel to the *ab*-plane of the interface resulted in orthorhombic final structures, and with final total energies higher than those corresponding to the structures depicted above. For example, for the 3-$SrTaO_2N$/3-$SrTiO_3$ SC, the energy difference between the trans-type N atoms parallel and perpendicular to the *ab*-plane resulted in 0.034 eV, which is greater than the precision of the calculation method. Then, only the *c*-ordered trans-type N atoms was considered.

4. Structural and electronic properties

In this section we present a summary of the main results obtained for the pure systems and then the study of the different SCs.

***-I4/mcm* STN.**

Input structures for *I*4/*mcm*-STN (space group 140) were constructed according to the experimental data from reference [3]. In this structure, the atomic Wyckoff positions are Ta 4*c*, Sr 4*b*, N 4*a* and O 8*h*. This last one has fractional coordinates (x, 1/2 + x, 0). The only degrees of freedom in the structure are *a*, *c* and *x*.

In table 1, *a*, *c*, and *x* parameters obtained after relaxation are presented. Both all-electron and pseudopotential approaches show a good agreement with the experimental data, although the cell volume, the oxygen *x* position, the Ta-O, Sr-O and Sr-N distances are closer to experimental data for QE calculations. We take this as a very good validation of the method and the pseudopotential selection.

***-Pm3m*, *I4/mcm* and *P4mm* STO.**

For bulk STO, calculations were performed in the cubic *Pm*3*m* phase (STOc) and in the tetragonal, both centro-symmetric (*I*4/*mcm*) and non-centro-symmetric phases (*P*4*mm*) (STOtc y STOtnc respectively). The obtained results are shown in table 1. For the cubic phase (STOc) the lattice constant after optimization resulted in a cell volume 2.6%

Table 1. Experimental and calculated lattice constants, volume, O x atomic positions and interatomic distances after full relaxation of the bulk STN and STO structures. The total energy for STO is referred to that of the STOc structure.

System	Method	a (Å)	c (Å)	Volume(Å^3)	O x	Ta − N(Å)	Ta − O(Å)	Sr − O(Å)	Sr − N(Å)	ΔE (eV)
	WIEN2k	5.586	8.2152	256.34	0.801	2.054	2.016	2.584	2.793	
	QE	5.643	8.218	261.66	0.796	2.055	2.028	2.621	2.821	
	Experimental	5.70251(6)	8.05420(16)	261.912(3)		2.01355(4)	2.019(5)			
STN *I*4/*mcm*	reference [3]									
	Experimental	5.7049(3)	8.0499(5)	261.99(4)	0.7721(4)	2.012	2.025	2.726	2.852	
	reference [37]									
	QE	3.939		61.12						0
STOc	Experimental	3.905		59.547						
	reference [19]									
STOtnc *P*4*mm*	QE	3.9285	3.9865	61.52						−0.0006
STOtc *I*4/*mcm*	QE	3.939	3.938	61.10						−0.0007

Table 2. Cell constants and ionic polarization obtained for the 3×3, 4×4 and 5×5 SCs after full relaxation of the atomic positions and cell constants. The numbering of the simple perovskite unit sub-cell starts with 1 just above/below the interface and increases as it moves up (for Ti sub-cells) or down (for Ta sub-cells) from it

Type	Cell	$\delta\vec{P}_{\text{ionic}}$ (10^{-3}C/m^2)	a (Å)	c (Å)	Type	Cell	$\delta\vec{P}_{\text{ionic}}$ (10^{-3}C/m^2)	a (Å)	c (Å)	Type	Cell	$\delta\vec{P}_{\text{ionic}}$ (10^{-3}C/m^2)	a (Å)	c (Å)
											Ti 5	7.9		3.871
						Ti 4	10.5		3.869		Ti 4	2.8		3.942
	Ti 3	12.6		3.863		Ti 3	3.5		3.935		Ti 3	2.8		3.950
	Ti 2	4.4		3.926		Ti 2	3.3		3.941		Ti 2	2.7		3.946
3×3	Ti 1	4.1	3.960	3.906	4×4	Ti 1	3.2	3.960	3.912	5×5	Ti 1	2.6	3.959	3.917
	Ta 1	3.9		4.416		Ta 1	3.0		4.422		Ta 1	2.4		4.430
	Ta 2	12.1		4.324		Ta 2	9.2		4.326		Ta 2	7.5		4.328
	Ta 3	12.5		4.354		Ta 3	9.3		4.327		Ta 3	7.5		4.326
						Ta 4	9.5		4.362		Ta 4	7.6		4.330
											Ta 5	7.97		4.365

higher than the experimental value. This fact lies within the normal overestimation of volume calculations using the GGA approximation. In the optimization of the lattice constants and atomic positions for the STOtc structure, the final a and c values were almost the same, resulting in a quasi-cubic cell, in very good agreement with the experimental value of a. Whereas, for the STOtnc, it was obtained a tetragonal distortion with $c/a = 1.015$ with the consequent displacements of cations and anions in opposite direction, that give rise to an electrical polarization. The total energy differences between the three structures are around 7×10^{-4} eV, which is not significant because such differences are within the calculation method error and moreover, it is well known that quantum fluctuations play an important role in $SrTiO_3$ preventing this compound to make a phase transition to a ferroelectric structure.

-*n*-$SrTaO_2N$/*n*-$SrTiO_3$ and V/*n*-$SrTaO_2N$/*m*-$SrTiO_3$ SCs.

Once the validation of the method was carried out on the pure compounds, the relaxations of the lattice constants and atomic coordinates of the SCs corresponding to the different *n*-$SrTaO_2N$/*n*-$SrTiO_3$ and V/*n*-$SrTaO_2N$/*m*-$SrTiO_3$ were performed. To analyze the internal behavior of the individual sub-cell units of the $SrBO_xN_y$ perovskites (B = Ti or Ta, $x + y = 3$), the lattice constants of the individual sub-cell were considered as those corresponding to the distance between the Sr atoms belonging to the same *ab*-plane for the case of the constant a_i^M, and to the distance between the Sr atoms of the adjacent planes for the case of the constant c_i^M (M indicates the shell M = STN or STO, and $i = 1, \ldots, n$) (see figure 1). In tables 2 and 3 it can be observed that, even starting from the initial configuration where for each side of the interface the individual cell constants a_i^M and c_i^M are equal for all i within each M, the result after the optimization is more complex. Due to the periodic boundary conditions, the constants a_i^M are equal for all i on both sides of the interface, obtaining an intermediate value of those corresponding to the STN and STO bulks. The obtained values are around 3.96 Å in close agreement with the reported value in reference [17] (3.98 Å). This result is encouraging and indicative that no defect formation or misfit dislocation has been formed in the samples. Then the STN layer is compressed while the STO layer is elongated, resulting in a compression strain for the first and a tensile strain for the second, as expected. This gives rise to a possible ferroelectric behavior in both layers, as will be analyzed later. In contrast, the c_i^M constants of the individual sub-cells after structural relaxation result in a more complex scheme that will be analyzed in the next section. Figure 3, shows the PDOS of the atoms for the SC V/4-$SrTaO_2N$/8-$SrTiO_3$ (V-4 × 8) case (the other structures show a similar behavior). Different shifts

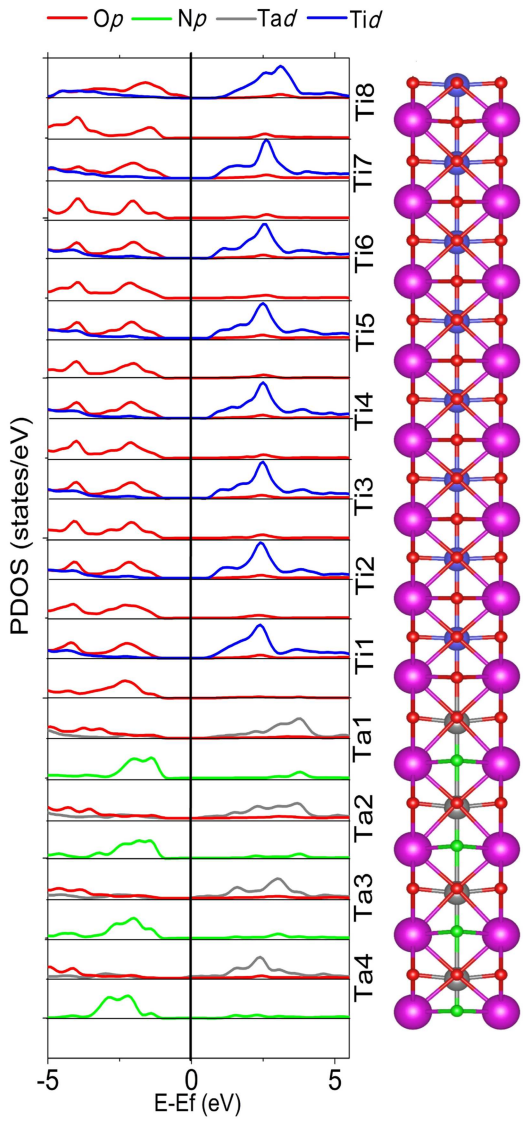

Figure 3. Partial density of states for Ta-d, Ti-d, O-p and N-p atoms calculated for the V-4 × 8 SC. The corresponding atoms are aligned with the graph. The energy scale is referred to the Fermi level.

of the electronic levels compared with the pure compounds can be observed. These shifts are multiple due to the different value of the resulting c_i^M constants and the local atomic rearrangement within each sub-cell. Previous studies on other heterostructures as $CaZrO_3/SrTiO_3$ [38, 39], and $AHfO_3/SrTiO_3$ [40] show polarization induced and two-dimensional electron gas behavior, strongly dependent on strain, layer stacking and thickness. The insulator-to-metal transition was reported to occur at thickness strongly dependent on surface termination. In the present study, no bands crossing the Fermi energy are observed for any of the different heterojunctions studied, suggesting that the presence of nitrogen prevents this type of behavior.

5. Polarization analysis

In this section the ionic and electronic contributions to the polarization are analyzed. For each SC, the ionic polarization of each sub-cell constituted by each individual perovskite cell structure was calculated.

It was not always clear how to calculate the polarization on a solid bulk, while studying a molecule or cluster with no net charge, it is defined straightforwardly as the separation of positive and negative charges in the system so that there is a net electric dipole moment per unit volume, where the ionic polarization is the one caused by relative displacements between positive and negative ions in ionic crystals.

With this definition in mind, and due to periodicity on bulk solids, the polarization on these systems is a multi-valued quantity, depending on the different choices of lattice vectors, that results in different ways of specifying the positions of the atoms. For each choice, a different polarization value is calculated, thus a lattice polarization can be defined instead of a polarization vector. If all the ions occupy positions with inversion symmetry, then that structure is non-polar.

Disagreements on how to calculate the polarization on solid bulks were ended with the so-called modern theory of polarization [29]. If the shape and/or size of the unit cell are changed the polarization lattice will also change, as for example in response to strain. So, the meaning of an experimental measurement of the spontaneous polarization is the change of the polarization between an initial and final state. This theory provides the following formula in order to calculate the ionic contribution to the polarization:

$$\delta\vec{p}_{\text{ionic}} = \vec{p}^{\,f} - \vec{p}^{\,0} = \frac{1}{V}\sum_i \left(q_i^f \mathbf{r}_i^f - q_i^0 \mathbf{r}_i^0\right), \qquad (1)$$

where q_i stands for the ionic charge of the individual atom located at $\mathbf{r}_i$. The f and 0 upper indexes refer to the final (polarized) and the initial (normally non-polar) lattice structures. Considering symmetry provided by periodic conditions, the sum must be performed over non-equivalent atoms.

5.1. Sub-cell ionic polarization

In the present study of $SrTaO_2N/SrTiO_3$ interfaces, in order to analyze the different contributions to the total polarization, the individual sub-cell ionic polarization is worth to be calculated. Still, care must be taken while applying the above stated formula. By construction, two different perovskite structures are matched together in order to generate the compound. Despite the whole SC is electrically neutral, this is not the case of each individual sub-cell. In particular, the sub-cells belonging to the interface have one N^{-3} atom in one face and an O^{-2} atom in the opposite face. After relaxation, due to tensile/constrain strain, each sub-cell ends up having a different volume: the same a_i for all sub-cells, but different c_i^M. This causes lack of periodicity in the c-direction. Moreover, the O, N and Ta/Ti atoms of the different octahedra move along the (001) direction different lengths. Thus, care must be taken for the individual sub-cell ionic polarization calculation due to the atoms on the lower ab-plane of each sub-cell are non-equivalent to those on the upper ab-plane. The ionic polarization of each sub-cell constituted by each individual perovskite cell structure was thus calculated as the difference between the

Table 3. Cell constants and ionic polarization obtained for the V-4 × 8 and V-5 × 10 SCs types SrO and SrN, after full relaxation of the atomic positions and cell constants. The numbering of the simple perovskite unit sub-cell starts with 1 just above/below the interface and increases as it moves up (for Ti sub-cells) or down (for Ta sub-cells) from it. The vacuum layer is also included.

Type	Cell	$\delta\vec{P}_{\text{ionic}}$ (10^{-3}C/m^2)	a (Å)	c (Å)	Type	Cell	$\delta\vec{P}_{\text{ionic}}$ (10^{-3}C/m^2)	a (Å)	c (Å)	Type	Cell	$\delta\vec{P}_{\text{ionic}}$ (10^{-3}C/m^2)	a (Å)	c (Å)	Type	Cell	$\delta\vec{P}_{\text{ionic}}$ (10^{-3}C/m^2)	a (Å)	c (Å)
											Vac.			13.749		Vac.			14.804
											Ti 9	0.3		4.057		Ti 9	−0.2		3.973
	Vac.			13.738		Vac.			13.923		Ti 8	0.4		3.964		Ti 8	0.0		3.896
	Ti 7	0.2		4.060		Ti 7	-0.2		4.062		Ti 7	0.5		3.940		Ti 7	0.1		3.897
	Ti 6	0.4		3.960		Ti 6	0.1		3.961		Ti 6	0.5		3.930		Ti 6	0.1		3.900
	Ti 5	0.4		3.937		Ti 5	0.1		3.934		Ti 5	0.5		3.925		Ti 5	0.0		3.895
	Ti 4	0.4		3.925		Ti 4	0.1		3.923		Ti 4	0.5		3.919		Ti 4	−0.0		3.877
V-4 × 8	Ti 3	0.4		3.921	V-4 × 8	Ti 3	0.1		3.917	V-5 × 10	Ti 3	0.5		3.919	V-5 x 10	Ti 3	−0.1		3.843
type SrO	Ti 2	0.4	3.954	3.911	type SrN	Ti 2	0.1	3.958	3.897	type SrO	Ti 2	0.4	3.956	3.908	type SrN	Ti 2	−0.1	3.959	3.813
	Ti 1	0.3		3.863		Ti 1	−3.6		3.827		Ti 1	0.4		3.864		Ti 1	−3.2		3.741
	Ta 1	−0.1		4.335		Ta 1	−3.3		4.290		Ta 1	0.0		4.339		Ta 1	−2.9		4.221
	Ta 2	3.6		4.245		Ta 2	−3.1		4.210		Ta 2	3.1		4.248		Ta 2	−2.7		4.154
	Ta 3	3.6		4.231		Ta 3	−3.1		4.194		Ta 3	3.1		4.240		Ta 3	−2.7		4.136
	Ta 4	3.4		4.150		Ta 4	−0.0		4.133		Ta 4	3.1		4.238		Ta 4	−2.7		4.125
											Ta 5	2.8		4.143		Ta 5	−0.1		4.062

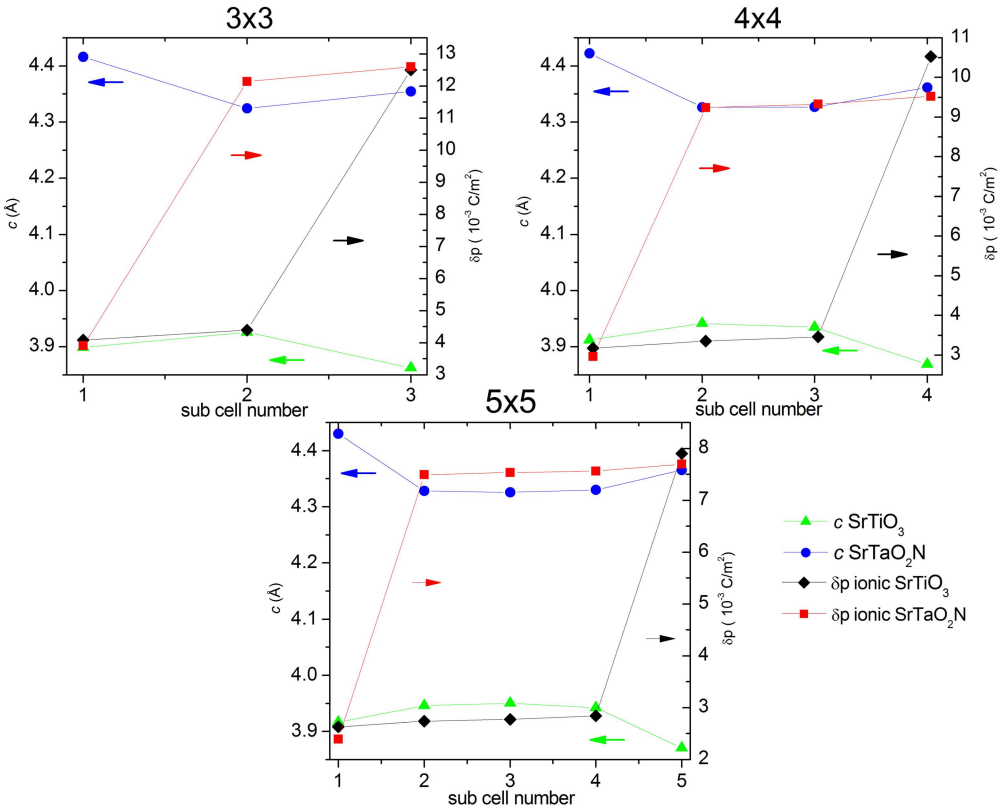

Figure 4. Sub-cell lattice constant c (left axis) and ionic polarization $\delta\vec{p}$ (right axis) calculated for the 3×3, 4×4 and 5×5 SCs. The arrows and colors indicate the corresponding vertical axis.

dipole moments of each sub-cell, after and before displacement from the symmetric position, as stated in equation (1). Before relaxation, $\vec{p}^{\,0} = 0$ in almost all sub-cells, except those two with non-zero net charge.

First, the positions of both the net positive and negative charge centers in every single sub-cell are found. The net positive final charge center position $\mathbf{r}^f_{q^+}$ is calculated by a weighted sum of the positions $\mathbf{r}^f_{i,q^+}$ of each individual cation in the sub-cell:

$$\mathbf{r}^f_{q^+} = \frac{\sum_i m_i w_i \nu_i \mathbf{r}^f_{i,q^+}}{Q^+_{\text{sub-cell}}}, \tag{2}$$

where the weight of each constituent is calculated by the multiplication of its valence charge ν_i, the fraction w_i (calculated by dividing the number of sub-cells that co-share this individual atom) and the multiplicity m_i of equivalent atoms within the sub-cell, divided by the total positive charge of the sub-cell $Q^+_{\text{sub-cell}}$. A similar formula is used to calculate all the others charge position centers, replacing initial positions instead of final positions, and negative charge positions $\mathbf{r}^f_{i,q^-}$ and $Q^-_{\text{sub-cell}}$ for the anions.

A net electric dipole structure oriented on the c direction is then formed, where the dipole displacement $\mathbf{d}^f = \mathbf{r}^f_{q^+} - \mathbf{r}^f_{q^-}$. Finally, the local ionic polarization is given by the dipole moment:

$$\vec{p}^{\,f} = \frac{q_e}{V_{\text{sub-cell}}}\mathbf{d}^f. \tag{3}$$

In the same way, $\vec{p}^{\,0}_{\text{ionic}}$ is calculated. It must be remarked that there is no additive relation among the ionic polarization on individual sub-cells and the total ionic polarization of the whole SC structure. This is so, because in each individual sub-cell both upper and lower *ab*-planes atoms, as they are non-equivalents, were taken into account, so all atoms in the *ab*-planes contribute to two different sub-cells, whereas in the total ionic polarization each *ab*-planes atoms must be counted only once.

-Multilayer *n*-$SrTaO_2$/*n*-$SrTiO_3$ ionic polarization.

In table 2 the results obtained for the c^M_i and the ionic polarization of each sub-cell in the systems *n*-$SrTaO_2$/*n*-$SrTiO_3$ (from here on $n \times n$) are presented. Each sub-cell has been labeled as Ta_i and Ti_i with $i = 1, \ldots, n$, being $i = 1$ the sub-cell corresponding to the central interface. All these SCs were built with the first sub-cell having a symmetric O octahedron at the Ti side of the interface (i.e. corresponding to a TiO_6 octahedron) and a non-symmetric O-N octahedron at the Ta side (corresponding to a TaO_5N octahedron) for $i = 1$. This geometry corresponds to the SrO termination-type. On the top and the bottom of the SC following the c axis, periodic boundary conditions form other interfaces with the inverted symmetry. For example, the 3×3 SC has a TiO_5N (non-symmetric) and a TaO_4N_2 (symmetric trans-type) octahedron at each side of the interface for $i = 3$. This corresponds to a SrN termination-type. In table 2, it can be observed that, for the Ti containing shells, the sub-cells present polarization values around 4.2×10^{-3} C m^{-2} for the 3×3, 3.3×10^{-3} C m^{-2} for

the 4×4 and 2.7×10^{-3} C m^{-2} for the 5×5 in those with symmetric octahedra ($i = 1, \ldots, n-1$), and a bigger ionic polarization around three times the one obtained before (12.1, 10.5 and 7.9×10^{-3} C m^{-2} respectively) at the non-symmetric sub-cell ($i = n$). In counterpart, for the Ta containing shell, the obtained polarization values are around 12.2×10^{-3} C m^{-2} for the 3×3, 9.3×10^{-3} C m^{-2} for the 4×4 and 7.5×10^{-3} C m^{-2} for the 5×5 for the symmetric trans-type sub-cells ($i = 2, \ldots, n$), with a decrease to around one third (3.9, 3.2 and 2.4×10^{-3} C m^{-2} respectively) for the non-symmetric sub-cell ($i = 1$). This behavior can be observed in figure 4. In this figure, the obtained values for the sub-cell lattice constant c_i^M are depicted on the left axis and those corresponding to the ionic polarization on the right axis. It can be observed that in the three cases the sub-cell constant c_1^{STN} results longer than the following in the same shell. This is due to the non-symmetry of the TaO_5N octahedron that produces an elongation of the corresponding sub-cell. On the opposite side, the last sub-cell in the Ti shell c_n^{STO} results shorter than the previous in the same shell, in this case for the non-symmetric TiO_5N octahedron.

-V/*n*-$SrTaO_2N$/*m*-$SrTiO_3$ ionic polarization.

For the V/*n*-$SrTaO_2N$/*m*-$SrTiO_3$ SCs (from here on V-4×8 and V-5×10), two different interface terminations were built: one with the octahedra pair TiO_6-TaO_5N (SrO-type), and the other with the octahedra pair TiO_5N-TaO_4N_2 at the interface (SrN-type). Total energy considerations show that the SrO-type are more stable than the SrN-type ($\Delta E = 7$ meV and 11 meV for V-4×8 and V-5×10 respectively). In table 3 and in figure 5 there are shown the results obtained for the c_i^M and the ionic polarization of the respective internal sub-cells. The results show that the polarization on each sub-cell on both Ti and Ta shells are much lower than those obtained for the multilayer $n \times n$ structures. This effect may be associated with the fact that the electric dipole coupling for the $n \times n$ multilayer occurs from the top and the bottom faces of the SC, having the multilayers two (different) interfaces per SC, while for the V-$n \times m$ SCs there is only one coupling interface. Also, no large decrease in the ionic polarization as a function to the distance to the interface is observed, suggesting a collective behavior in each shell. The quasi-null value for the polarization for the last sub-cell Ta_n in the SrN interface-type structure is due the lack of symmetry of the last TaO_5N octahedron. This fact is a requirement for charge neutrality considerations.

Comparing the ionic polarization between SrO and SrN interface-type structures, large differences can be observed: the ionic polarization resulted much lower in the Ti containing shells for SrN interface-type, due to the non-symmetric first TiO_5N octahedron. Also, the way to initialize the Ta layer affects the sign of the resulting polarization: in SrN interface-type cells, the Ta shells present polarization values with the opposite sign than that of the Ti shells, while for the SrO interface-type, the individual sub-cell polarization are in the same direction. It should be noted that the sub-cell ionic polarization is lower for SrN interface-type comparing to the corresponding SrO one, and for the Ti containing shell for the SrN interface-type is nearly null for the V-5×10 SC.

Another outstanding aspect in the analysis of the origin of the electric dipolar moment arises from the comparison of the individual ion displacement outside the central-symmetric positions. In the ferroelectric space group *P*4*mm* phases bulk ABO_3 perovskites, the dipole moment arises from the displacement in opposite directions of the central B cation and the O anions along the direction of the axis *c* (in this representation, taking the A atoms position as the cell boundaries, and the *ab*-plane at $c/2$ as the symmetry plane). In contrast, for the present systems, a different behavior of the displacements of anions and cations is observed. Figure 6 shows a projection of the atomic positions on the *bc*-plane before and after the structural relaxation in the 5×5 multilayer SC. As mentioned, the starting structures were built with centro-symmetric positions for the Ti layers, and non-centro-symmetric positions for Ta layers, with a small initial displacement in one direction of the Ta cations (down from the central plane in figure 6). After the resulting atomic rearrangement due to relaxation, the Ta moves upward, now occupying positions slightly above the central symmetry plane, and the oxygen and nitrogen atoms move away in the same direction. This configuration results in a net dipole moment but based on different displacement lengths of cations and anions in the same direction. Also in figure 6 it can be observed that the only exception occurs in the first sub-cell of Ta corresponding to the interface, due to the asymmetry of the TaO_5N octahedron, in which the Ta remains slightly below the plane of symmetry, and the anions move above it. The individual sub-cell polarization at the Ti layer side presents a similar behavior for some sub-cells (Ti 4–5 in figure 6) but not for all of them. Nevertheless, the local sub-cell polarization has the same sign in the five cases Ti 1–5. It should be mentioned that in order to ensure that the final atomic configurations have not fallen within a local energy minimum, different paths were taken to optimize the initial structures, resulting in similar final endpoints for all the pathways for each SC studied. In the supplementary information the whole atomic positions and cell parameter are given.

5.2. Total polarization

Finally, the total (i.e. ionic plus electronic) polarization was computed for the optimized structures. For the calculations, both the modern theory of polarization by means of the Berry phase concept was used following the guidelines in the work of Spalding [41], and also the Born's effective charge tensor were computed [30, 31]. As in the previous subsection, for the calculation of $\delta\vec{p} = \vec{p}^{\,f} - \vec{p}^{\,0}$, we defined the initial phase to that one built from the final relaxed structure by displacing the apical O/N atoms *z* position in each octahedron to that of the corresponding Sr atoms plane, together with the displacement of the central Ta/Ti and O atoms *z* position to the midpoint of the upper and lower Sr atoms plane. In this way we can vary continuously the atomic positions toward the final structure by means of a unique parameter λ that runs from 0 to 1 and calculate the polarization variation as:

$$\delta\vec{p} = \int_0^1 \frac{\mathrm{d}\vec{p}}{\mathrm{d}\lambda}\mathrm{d}\lambda. \tag{4}$$

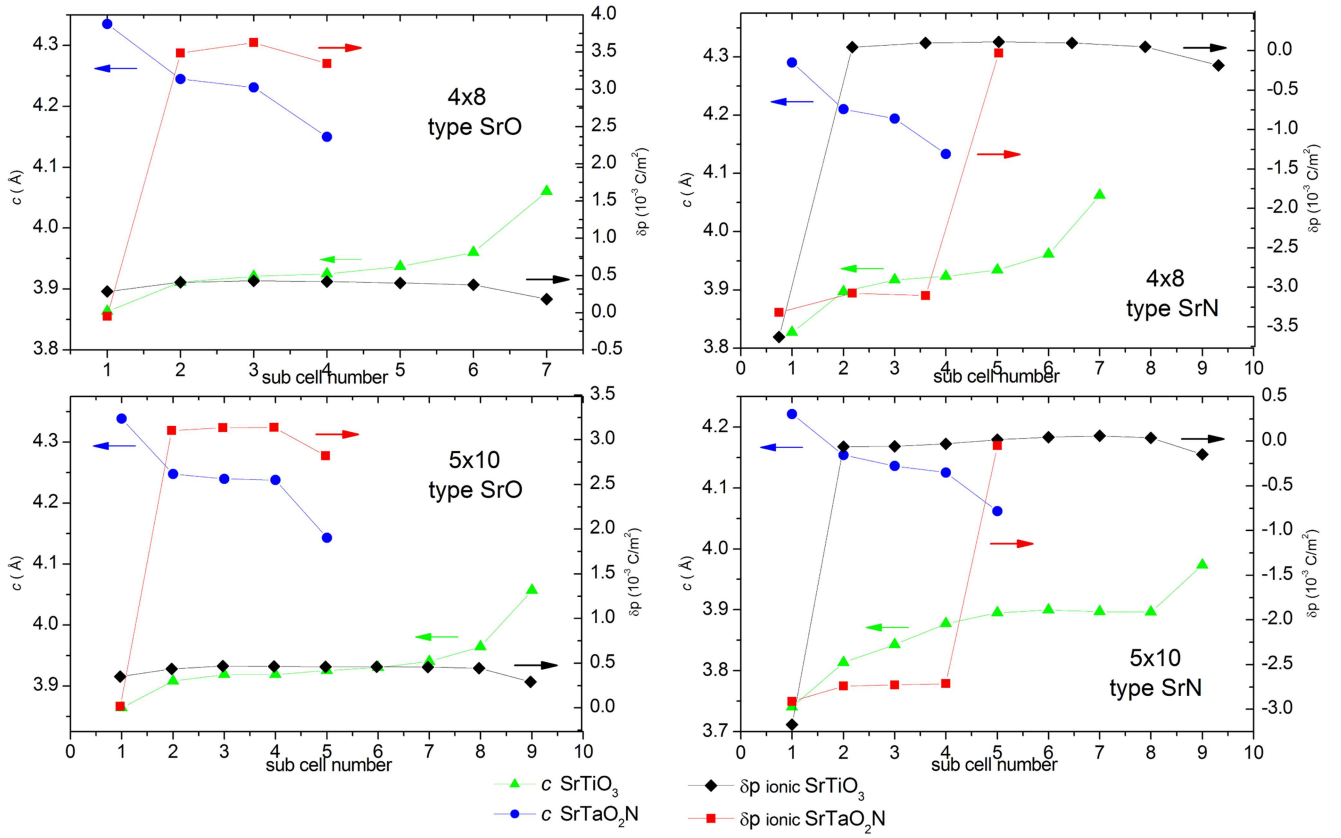

Figure 5. Sub-cell lattice constant c (left axis) and ionic polarization $\delta\vec{p}$ (right axis) for the V-4 $\times$ 8 and V-5 $\times$ 10 (SrO and SrN-type) SCs.

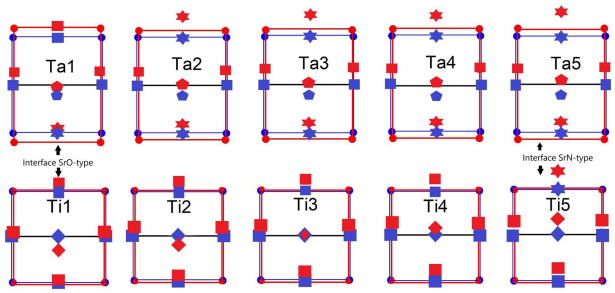

Figure 6. Projection onto de bc-plane of the atomic positions and lattice constants before (blue) and after (red) atomic positions and cell relaxations in the 5 $\times$ 5 SC. The atomic symbols are Sr (circle), Ta (pentagon), O (square), N (star) and Ti (rhombus).

Within this method, the two types of contributions to the polarization are calculated separately:

$$\Delta\vec{P} = \delta\vec{p}_{\text{ionic}} + \delta\vec{p}_{\text{electronic}}, \tag{5}$$

and as a direct consequence, each component of the ionic and electronic polarization is defined except for a multiple of the corresponding component of the quantum of polarization:

$$\frac{q_e}{V_C}\vec{R} = \frac{q_e}{V_C}(\vec{a}_1 + \vec{a}_2 + \vec{a}_3), \tag{6}$$

where q_e is the electron charge, V_C is the cell volume and the $\vec{a}_i$ are the vectors of the Bravais network of the structure associated with V_C.

Due to the above-mentioned multi-valued characteristic of the polarization, attention must be taken when going from one structure to the other in order to calculate the polarization variation $\Delta\vec{P}$, in that the initial and final values correspond to the same branch. So, for each $n \times n$ SC, 10 intermediate structures were prepared, starting with the initial structure ($\lambda = 0$) and approaching gradually the final structure ($\lambda = 1$) by increasing λ in $1/11$ steps. Also, polarization quanta were calculated for each structure. In this way we could identify and/or correct the calculated intermediate values in order to ensure they belong to the same branch. In figure 7 the obtained results are shown for three different branches for each $n \times n$ SC.

Born's effective charge is a tensor that relates the macroscopic polarization component in each x_i direction with the collective displacement of a type-k atom in the x_j direction:

$$Z_{kij} = V\left.\frac{\partial P_i}{\partial x_{kj}}\right|_{\vec{E}=0}, \tag{7}$$

where V is the volume of the cell, and $\vec{E}$ is the macroscopic electric field. The effective Born's charge of a given atom is a dynamic load in the sense that represents the polarization response of a given type of atomic displacement:

$$\Delta P_i \cong \frac{1}{V}\sum_{k=1}^{N}\sum_{j=1}^{3} Z_{kij}\Delta x_{kj}. \tag{8}$$

In the last expression, Δx_{kj} represent the atomic displacements from the initial to the final structures.

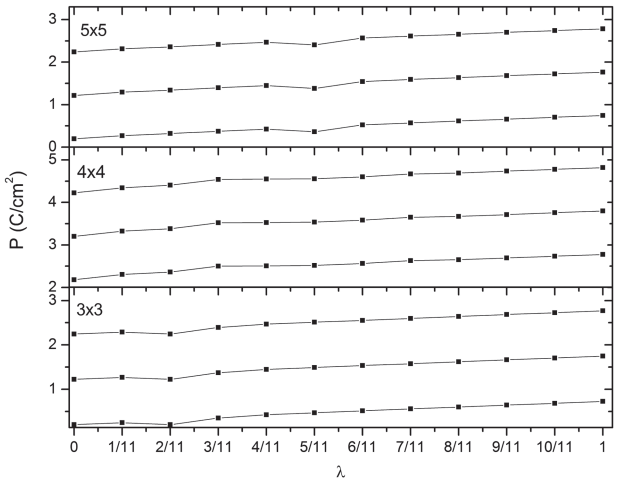

Figure 7. Total polarization as a function of the order parameter λ for the 3×3, 4×4 and 5×5 SCs. The graphs show the increment of the calculated P by varying quasi continuously λ form the initial structure ($\lambda = 0$) to the final structure ($\lambda = 1$). Three contiguous branches are plotted separated by the corresponding quantum of polarization in the *c*-direction.

Table 4. Total polarization for the different relaxed *nxn* and V-*mxn* SCs obtained using the modern theory of polarization by the Berry phase method and the Born's effective charges tensor method.

Type of super cell	Berry phase method(Cm^{-2})	Born′s effective charges tensor method (Cm^{-2})
3×3	-0.52	-0.51
4×4	-0.59	-0.49
5×5	-0.54	-0.49
V-4×8		-0.029
V-5×10		-0.039

The obtained results for $\Delta\vec{P} = \delta\vec{p}_{\text{ionic}} + \delta\vec{p}_{\text{electronic}}$ in the (001) direction are presented in table 4. For the $3 \times 3, 4 \times 4$ and 5×5 multilayer structures, the polarization is around -0.5 C m^{-2}, while for the unique-interface structures V/4-$SrTaO_2N$/8-$SrTiO_3$ and V/5-$SrTaO_2N$/10-$SrTiO_3$ the corresponding values are lower: ~ -0.029 and -0.039 C m^{-2} respectively. As a reference point, they should be compared with the corresponding to the well-known ferroelectric $BaTiO_3$, ≈ 0.26 C m^{-2}. This result is encouraging for the development of this type of multilayer structures and the techniques for fabrication. Also, it can be observed a very good agreement in the polarization values obtained by two very different calculation methods for the multilayer $n \times n$ structures. For the V/*n*-$SrTaO_2N$/*m*-$SrTiO_3$ structures the presence of the vacuum layer makes the calculation of the polarization by the Berry phase method very difficult to obtain with a good convergence, so they were discarded and only those obtained by the Born's effective charges method are shown. An additional advantage of the Born's effective charge calculation is that it provides the individual atomic contribution to the total polarization. The individual obtained values are included in the supplementary information. It is observed that, for the $n \times n$ multilayer structures, the principal contribution arises from the Ta and Ti with asymmetric octahedra (TaO_5N and TiO_5N), the Ti and Ta with symmetric TiO_6 and TiO_4N_2 at the interface, the N atoms, and the O atoms corresponding to the intermediate Ti octahedra (i.e., not belonging to an interface). On the other hand, for the V-4×8 and V-5×10 single interface structures, the major contributions come from the Ta atom at the interface, the single N at the vacuum surface, the O atoms at the interface, and the apical O atoms of the intermediate TiO_6 octahedra.

Thus, this result is encouraging. The macroscopic polarization results similar for the three SCs under study. According to our knowledge this type of multilayer cells has not yet been fabricated. Although the difference in network constants between $SrTiO_3$ and $SrTaO_2N$ is a bit large, the simple interface has been successfully constructed in the cited experimental works. Thus, it can be expected that this type of periodic structure can also be manufactured. The results show that its development can be of great interest. In the case of the V/*n*-$SrTaO_2N$/*m*-$SrTiO_3$ structures, this last cell format is close to the experimental studies on thin film STN deposited on STO substrate. Although the value obtained for the total polarization is lower than in the case of multilayers, it was not zero, thus, the results presented in this work supports the experimental results presented in the work of Oka *et al* [17].

6. Summary and conclusions

In this work we have analyzed the spontaneous rupture of inversion symmetry in two naturally dielectric compounds under normal conditions by the strain produced by the formation of a heterostructure. The determined net polarization appears as a consequence of the compression/tension stress that naturally arises between them under epitaxial growth due to the mismatch between their lattice constants. Different possible configurations were analyzed: the multilayer structure, and an approximation to a thin unique interface scheme. As a result of the proposed models, it was observed that the induced electrical polarization strongly depends on the termination layer at the interface, according to the content of oxygen or nitrogen atoms at the separation plane. The atomic displacement in each individual sub-cell was analyzed in detail, showing that the distortions that lead to electric polarization are not identical in each sub-cell, and that the displacement of anions and cations in the epitaxial direction does not follow the conventional scheme for phases with *P*4*mm* symmetry in perovskites. Finally, the total electric polarization was calculated, resulting for the multilayer structures in greater values than that of the reference compound $BaTiO_3$, leading to an open field to further experimental studies and a strong interest in the studied systems from the point of view of their possible industrial applications.

Acknowledgments

This work was partially supported by Consejo Nacional de Investigaciones Científicas y Técnicas (CONICET) under Grants PIP11220170100987CO and

PIO15520150100001CO, Facultad de Ingeniería, Universidad Nacional de La Plata under Grant I191 and Facultad de Ciencias Exactas, Universidad Nacional de La Plata under Grant X843. We also thank the computational centers CSCAA, Aarhus Universitet, Denmark, and Proyecto Acelerado de Cálculo of the SNCAD-MINCyT, Argentina. Also, to the Instituto de Física La Plata-CONICET, Argentina, for the use of its facilities. Finally, to Dra. M A Taylor and L A Errico for careful reading and inspiring discussions.

ORCID iDs

V I Fernández https://orcid.org/0000-0003-0371-9611

References

[1] Kim S, Kang T S and Je J H 1999 *J. Mater. Res.* **14** 2905–11
[2] Jansen M and Letschert H P 2000 *Nature* **404** 980–2
[3] Kim Y I, Woodward P M, Baba-Kishi K Z and Tai C W 2004 *Chem. Mater.* **16** 1267–76
[4] Kasahara A, Nukumizu K, Hitoki G, Takata T, Kondo J N, Hara M, Kobayashi H and Domen K 2002 *J. Phys. Chem.* A **106** 6750–3
[5] Yang M, Oró-Solé J, Kusmartseva A, Fuertes A and Attfield J P 2010 *J. Am. Chem. Soc.* **132** 4822–9
[6] Marchand R and Laurent Y 1984 *FR Pat* 17274
Marchand R and Laurent Y 1985 *Eur Pat* 402155-7*, French and European Patents*
[7] Marchand R, Pors F, Laurent Y, Regreny O, Lostec J and Haussonne J M 1986 *J. Phys. Colloq.* **47** C1-901–5
[8] Pors F, Marchand R, Laurent Y, Bacher P and Roult G 1988 *Mater. Res. Bull.* **23** 1447–50
[9] Marchand R, Laurent Y, Guyader J, L'Haridon P and Verdier P 1991 *J. Eur. Ceram. Soc.* **8** 197–213
[10] Shannon R D 1993 *J. Appl. Phys.* **73** 348–66
[11] Halasyamani P S and Poeppelmeier K R 1998 *Chem. Mater.* **10** 2753–69
[12] Bersuker I B 2001 *Chem. Rev.* **101** 1067–114
[13] Burdett J K 1995 Chemical bonding in solids *Topics in Inorganic Chemistry* (New York: Oxford University Press)
[14] Page K, Stoltzfus M W, Kim Y I, Proffen T, Woodward P M, Cheetham A K and Seshadri R 2007 *Chem. Mater.* **19** 4037–42
[15] Yang M, Oró-Solé J, Rodgers J A, Jorge A B, Fuertes A and Attfield J P 2011 *Nat. Chem.* **3** 47–52
[16] Zhang Y R, Motohashi T, Masubuchi Y and Kikkawa S 2011 *J. Ceram. Soc. Japan* **119** 581–6
[17] Oka D, Hirose Y, Kamisaka H, Fukumura T, Sasa K, Ishii S, Matsuzaki H, Sato Y, Ikuhara Y and Hasegawa T 2014 *Sci. Rep.* **4** 4987
[18] Zhu W, Kamisaka H, Oka D, Hirose Y, Leto A, Hasegawa T and Pezzotti G 2014 *J. Appl. Phys.* **116** 053505
[19] Haeni J H *et al* 2004 *Nature* **430** 758–61
[20] Alonso R E, Taylor M A, Gil Rebaza A V, Cappelletti M and Fernández V 2018 *Bol. Soc. Esp. Ceram. Vidrio* **57** 40–4
[21] Hinuma Y, Moriwake H, Zhang Y R, Motohashi T, Kikkawa S and Tanaka I 2012 *Chem. Mater.* **24** 4343–9
[22] Kohn W and Sham L J 1965 *Phys. Rev.* **140** A1133–8
[23] Giannozzi P *et al* 2009 *J. Phys.: Condens. Matter* **21** 395502
[24] Perdew J P, Burke K and Ernzerhof M 1996 *Phys. Rev. Lett.* **77** 3865–8
[25] Vanderbilt D 1990 *Phys. Rev.* B **41** 7892–5
[26] Monkhorst H J and Pack J D 1976 *Phys. Rev.* B **13** 5188–92
[27] Lehmann G and Taut M 1972 *Phys. Status Solidi* (*b*) **54** 469–77
[28] Sanchez-Portal D, Artacho E and Soler J M 1995 *Solid State Commun.* **95** 685–90
[29] King-Smith R D and Vanderbilt D 1993 *Phys. Rev.* B **47** 1651–4
[30] Neaton J B, Ederer C, Waghmare U V, Spaldin N A and Rabe K M 2005 *Phys. Rev.* B **71** 014113
[31] Roy A, Prasad R, Auluck S and Garg A 2010 *J. Phys.: Condens. Matter* **22** 165902
[32] Sjöstedt E, Nordström L and Singh D J 2000 *Solid State Commun.* **114** 15–20
[33] Madsen G K H, Blaha P, Schwarz K, Sjöstedt E and Nordström L 2001 *Phys. Rev.* B **64** 195134
[34] Cottenier S 2002 *Instituut Voor Kern-En Stralingsfysica* (Belgium: KU Leuven) vol 4
[35] Blaha P, Schwarz K, Madsen G, Kvasnicka D and Luitz J 2001 WIEN2k: An Augmented Plane Wave plus Local Orbitals Program for Calculating Crystal Properties Technische Universität Wien (Wien)) vol 28
[36] Uberuaga B P, Dholabhai P P, Pilania G and Chen A 2019 *Apl. Mater.* **7** 100904
[37] Günther E, Hagenmayer R and Jansen M 2000 *Z. Anorg. Allg. Chem.* **626** 1519–25
[38] Nazir S, Cheng J and Yang K 2016 *ACS Appl. Mater. Interfaces* **8** 390–9
[39] Chen Y *et al* 2015 *Nano Lett.* **15** 1849–54
[40] Cheng J, Nazir S and Yang K 2016 *ACS Appl. Mater. Interfaces* **8** 31959–67
[41] Spaldin N A 2012 *J. Solid State Chem.* **195** 2–10